JAAS FULL PAPER
www.rsc.org/jaas

Vaporization process of SiO_2 particles for slurry injection in inductively coupled plasma atomic emission spectrometry

H. B. Lim,*[a] T. H. Kim,[a] S. H. Eom,[a] Yong-ik Sung,[a] M. H. Moon[b] and D. W. Lee[c]

[a]*Department of Chemistry, Dankook University, Youngsan-ku, Hannam-dong Mt. #8, Seoul 140-714, Republic of Korea*
[b]*Department of Chemistry, Pusan National University, Pusan 609-735, Republic of Korea*
[c]*Department of Chemistry, Yonsei University, Seodamunku, Yonhee-dong, Seoul 120-749, Republic of Korea*

Received 3rd September 2001, Accepted 11th December 2001
First published as an Advance Article on the web 11th January 2002

In this work, the vaporization process of SiO_2 particles in an ICP was theoretically and experimentally investigated. The emission intensity of Si I for the three different sizes of SiO_2 particles, 0.35, 1.4 and 2.5 μm, was measured as the observation height varied. Based on these experimental heights, the heat-transfer and mass-transfer models were applied in order to understand the vaporization process of SiO_2 particles in an ICP. When a heat-transfer-controlled model is considered for the process, the rate for a SiO_2 particle in the tested size became comparable to that obtained by experiment. SiO_2 particles in the range of 0.3–2.6 μm seemed to be vaporized by a heat-transfer-controlled mechanism, rather than by a Knudsen-effect-corrected heat-transfer-controlled or mass-transfer-controlled mechanism in an atmospheric pressure ICP.

Introduction

Slurry nebulization offers a lot of advantages over conventional dissolution techniques, being simpler, less time-consuming as there is no sample pretreatment, and less prone to the possibility of contamination.[1–5] Because finely divided powders are inserted into the plasma, the size of the slurry particle affects the accuracy of the analytical measurement *via* two processes: the possible alteration of the composition of a sample during transport into the plasma and the possible bias in the measurement response.[6,7] Reportedly, measurable differences between slurries and solutions of not only refractory elements but also non-refractory elements have been observed for totally transportable slurries.[8] Slurries having a particle size of <1.5 μm have been reported to behave like aqueous solutions in a standard torch ICP-AES.[7,9] The deviation of intensity of particles >2 μm from that of aqueous solutions was due more to the interaction of refractory particles with the plasma than to interference effects in the sample transport and introduction system.[9]

Recently, the behaviour of slurry particles in the plasma has been investigated to discover how this behaviour affects the analytical result. Several workers have investigated the mechanism of desolvation and vaporization of solute particles or sample droplets in a flame spectrometer. Raeymaekers *et al.* described the evaporation of solid particles by using a simple physical model and compared the results to experiments performed with Al_2O_3 and SiO_2 slurries.[2] From that work, they found that the nebulization characteristics for suspensions were similar to those of solutions and only particles with a diameter below 17 μm reached the ICP. The above work used various particles supplied by companies, in which size was relatively distributed in a wide range. The evaporation efficiency was found to be 70–75% for a 0–10 μm particle, and about 20% for a 10–20 μm particle with respect to the calculated degree of evaporation and was stabilized at about 20 mm above the load coil.

The rate and extent of particle vaporization with spatial and temporal resolution of the events in a flame were investigated by Hieftje and co-workers[10,11] in order to determine the various factors that influence the time-dependent production of free atoms. For this, two alternative models, heat-transfer and mass-transfer, were developed and mathematical expressions were derived for the calculation. Clampitt and Hieftje[12] described a method of calculation for the high temperature thermal parameters required for examination of the desolvation mechanism of flame spectrometric solvent droplets. For the desolvation processes, an extended model was developed, which provided excellent correlation between the theoretical and experimental rates of desolvation.

Recently, Horner and Hieftje studied the mechanism of matrix interference by incorporating the droplet desolvation and solute particle vaporization processes using computer simulation.[13] Even though neither model successfully predicted the entire history of a large solute mass in the vaporization process, theory and experiment showed a change in behavior as the particle reached sub-μm size. From this study, they found that mass-transfer-controlled vaporization was preferable for a small particle, and heat-transfer was favorable for a large particle. Therefore, particle size is one of the important factors affecting the vaporization process.

In this work, we investigated the vaporization process of a SiO_2 particle in the ICP by measuring observation height. Since there are various size ranges of particulate material, a narrow size distribution was required to elucidate the effect of particle size on the vaporization process: micron-sized SiO_2 particles sample were fractionated into particles of various diameters by using split-flow thin fractionation (SPLITT fractionation or SF technique). SPLITT fractionation is a rapid and continuous separation technique for separating colloidal and particulate matter.

Separation of particles in SPLITT is carried out in a thin ribbon-like channel having flow splitters at both ends.[14,15] In a SPLITT channel there are two inlets and outlets where the suspended particle solution is continuously fed into one inlet and the carrier flow liquid is introduced through the other inlet. During the migration of particles along the channel, particles are driven toward one of the channel walls by an external force (gravity for gravitational SPLITT system), which acts perpendicularly to the direction of flow. Thus, separation takes place across the channel according to the particle size or mass and is normally achieved very quickly due to the thinness of

the channel. Even though there are only few separation techniques that have been developed and employed for the separation of particulate materials, *e.g.*, gravity-driven elutriation, air classification and a number of centrifugal techniques, resolution of the first is restricted due to a non-uniform flow profile and the last requires a tedious layering of density gradients to overcome convective perturbations. Compared to these conventional techniques, SPLITT has the capacity to separate particulate materials in a continuous, efficient operation.[16–18]

In our experiments, SiO_2 particles separated in size by SPLITT were introduced by slurry nebulization, and the intensity changes after variation of the observation height in an ICP were measured. Assuming the height corresponds to the vaporization time, the heat-transfer and mass-transfer models described by Hieftje and co-workers[10,11] were used to understand the vaporization mechanism.

Experimental

Instrumentation

The instrument employed in this study was a Jobin–Yvon 138 (JY 138, France) high-resolution nitrogen-purged monochromator ICP-AES; the wavelength for Si was 212.412 nm. This system is equipped with a 40.68 MHz generator with a standard side-view torch including a sheath gas flow and a 1 m focal length monochromator. It was operated at 1.0 kW forward power with a coolant flow of 12 l min^{-1} and a sample uptake rate of 1.7 ml min^{-1} obtained with a peristaltic pump (Minipuls 3, Gilson®, France). The sheath gas flow was omitted throughout this work. Observation height was varied as necessary. A slit mask with 1 mm height was placed in front of the slit with a width of 20 μm to observe the analyte emission.

The slurry sample was delivered to an MDSN (maximum dissolved solid nebulizer, ARL Co.) through the 1.2 mm id tubing for a standard torch ICP-AES.

Particle size measurement of SiO_2 powder

Particle size was measured by using a particle size analyzer (HELOS, Sympatec GmbH, Germany). A suspension of about 1% (w/v) of sample powder in a sodium phosphate dispersant was homogenized by ultrasonic vibration for 10 min and agitated with a magnetic stirrer. Subsequently, the sample was pumped in a circuit through a cuvette and a laser beam was scattered on the particles. The particle size distribution was directly obtained.

Another method of estimating the particle size after SPLITT is to use a scanning electron microscope (SEM). In this experiment scanning electron micrographs of sample powders were obtained using a scanning electron microscope (JSM-5200, Jeol, Japan) and compared with the results of the particle size analyzer.

Slurry sample preparation

Slurries containing about 0.1% (w/v) suspended SiO_2 powder (325 mesh, 99.6%, Sigma–Aldrich, USA) were prepared by transferring SiO_2 quantitatively into a 100 ml polyethylene flask and adding deionized water to the mark. The desired pH was attained by adding either HCl or NH_4OH. The high purity chemicals were obtained from DongWoo Pure Chemical Co., Ltd. (Ik-San, Republic of Korea). Sodium dodecyl sulfate (Sigma–Aldrich) of 0.01% (w/v) was used as a surfactant to stabilize the slurries, if necessary. The slurry was ultrasonically treated for 30 min before being introduced into the plasma, in order to destroy agglomerates and sufficiently stabilize the slurries. Slurry homogeneity can be maintained during delivery by continuous mechanical stirring and confirmed using SEM.

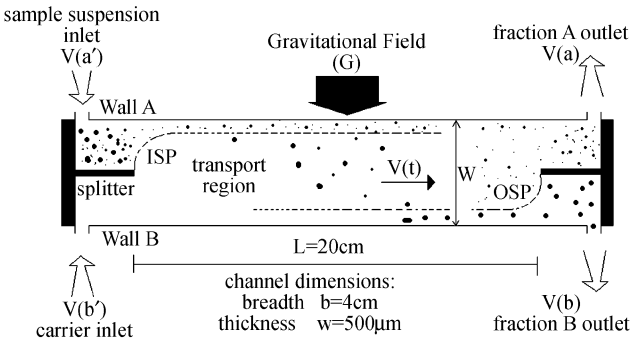

Fig. 1 Side view of SPLITT channel.

Particle separation

Separation in SPLITT takes place in a thin (300–800 μm) ribbon-like rectangular channel with splitter plates located at the beginning and end of the channel, as shown in Fig. 1. Suspended particles are introduced along the feed stream through the upper inlet, a', and the carrier flow is introduced from the bottom inlet, b'. Since the carrier flow from the bottom inlet is normally adjusted to be faster than the feed stream, particles fed into the channel are pushed toward the upper wall of the channel and migrate toward the end of the channel. Simultaneously, a driving force (external field) is applied to particles in a direction perpendicular to the flow axis; migrating particles migrate differentially along the transverse direction based on their characteristic transport coefficients. When a gravity field is used in gravitational SPLITT, particles settling slowly will exit toward the upper outlet, a, and those that settle quickly will exit toward the bottom outlet, b. Thus, in gravitational SPLITT, collected particles in both outlets are enriched/depleted within a certain range of particle size, which is adjusted by controlling the two outlet flow rates.

Results and discussion

Particle separation by SPLITT

In order to study the effect of particle size on the vaporization process for slurry injection in ICP-AES, three different diameters of slurry particles, >4.17 μm, 0.76–2.55 μm and <0.76 μm were prepared using a lab-made SPLITT system, shown in Fig. 2. The particle diameters were found using the following equation:[16,17]

$$dc = \sqrt{\frac{18\eta[V(a) - 0.5V(a')]}{bLG\Delta\rho}}, \quad (1)$$

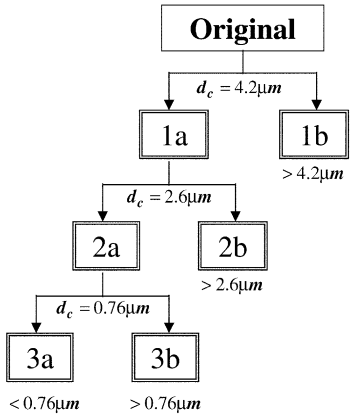

Fig. 2 Sequence of SPLITT fractionation separation.

Table 1 Experimental flow rate conditions for SPLITT fractionation of silica particles according to each cutoff diameter, d_c

d_c /μm	V(a')/ ml min^{-1}	V(b')/ ml min^{-1}	V(a)/ ml min^{-1}	V(b)/ ml min^{-1}
4.2	1.0	8.0	8.0	1.0
2.6	0.4	3.0	3.0	0.4
0.76	0.1	0.3	0.3	0.1

where b is the channel breadth of 4 cm, L is the channel length of 20 cm, η is the viscosity of the carrier solution, 0.01 g s cm^{-1}, G is the gravitational field, $\Delta\rho$ = 1.65 g cm^{-3} is the density difference between the carrier field and particles, V(a') is the top inlet flow rate, V(a) is the top outlet flow rate, and V(t) is V(a)$-V$(a'). From the equation, the cut-off diameter, d_c, in a gravitational SF is found to be proportional to flow rates and other experimental parameters. Therefore, using the physical parameters given above, the expected particle diameters were calculated as the inlet and outlet flow rates were varied, as shown in Table 1.

The mass mean diameters for particles separated in this experiment were calculated as: 0.31 μm for $<$0.76 μm; 1.6 μm for 0.76–2.6 μm; and 4.4 μm for $>$4.2 μm. However, in order to measure the diameters accurately, SEM pictures were taken (shown in Fig. 3). The measured mean diameters for the three groups obtained from the pictures were 0.35, 1.4 and 2.5 μm, respectively. The separated particles were homogeneously distributed in size and matched the expected values with some deviation. In this study measured particle diameters obtained using SEM pictures were used.

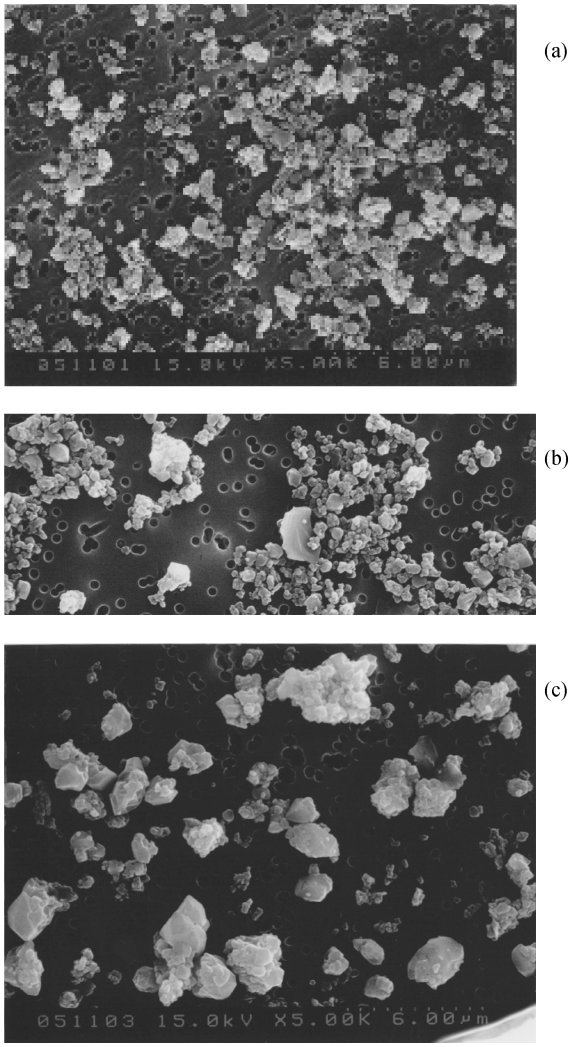

Fig. 3 Pictures of SiO_2 particles separated by SPLITT: (a) 0.31 μm cut-off diameter, (b) 1.6 μm and (c) 4.4 μm.

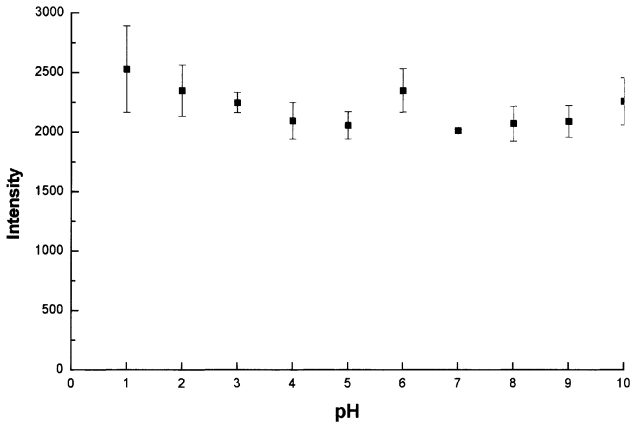

Fig. 4 Dependence of slurry stability of Si I on pH.

Dispersion of prepared particles

The important factors in particle dispersion are known to be particle size and the stability of the slurries. A stable dispersion is related to the homogeneity of the slurry and leads to the production of reproducible analytical results. Even though the particles can be well-dispersed in a beaker by simply using mechanical stirring or ultrasonification, aggregation and flocculation of the particles may be observed during delivery of the slurries through the Tygon tubing of a peristaltic pump if no dispersant is used. Since pH is known to affect stable suspension,[19–22] emission intensity and its relative standard deviation were measured while the pH of the slurry was varied. Experimental results of the dependence of suspension stability on pH are shown in Fig. 4. The variation of Si I (212.412 nm) intensity and its relative standard deviation with pH was not severe, unlike Fe_2O_3 and Al_2O_3. At a low pH of 1 or 2 and a high pH of over 11, the standard deviation increased. The signal-to-noise ratio was almost unchanged in the range of pH 3–9. In our experiment, therefore, the slurry was maintained at pH 8 without using dispersants. At this pH level, no particle aggregation or flocculation was observed in the Tygon tubing of the peristaltic pump. The slurries for each particle range were prepared at a concentration of about 0.1% as described above.

Observation height measurement

Since the height (H) in the plasma at which a solute particle is completely vaporized has an approximately linear relationship with the initial diameter (d) of the particle, a linear relationship to the central channel flow rate (v), and an inverse relationship to the forward power (p)[13] and other physical and chemical parameters (u), it can be expressed by the following:

$$H = f(d, v, 1/p, u) \quad (2)$$

If the particle size is large, more time for complete vaporization is required and a larger H will be expected. Alternatively, earlier vaporization of small particles shifts the observed analyte emission and fluorescence curves downward along the axis of the ICP and, therefore, allows more time for diffusion and a small H.

In our experiments, the emission intensity of Si I for three kinds of SiO_2 particles, separated by SPLITT, was measured three times as the observation height was varied. The result for a 2.5 μm particle is shown in Fig. 5. As shown in this figure, the intensity increased continuously as the observation height increased and reached a maximum at 14.2 mm. Since the entire cross section of the plasma was not viewed in this experiment,

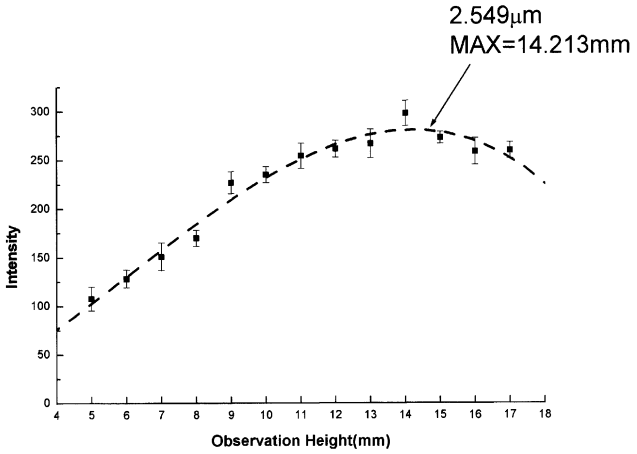

Fig. 5 Intensity change of 2.5 μm SiO_2 particles in ICP-AES as a function of the observation height.

the atomization curve may be influenced by various factors, such as diffusion, ionization, *etc.* If these factors are assumed to be relatively small compared to atomization of the SiO_2 particle, the position showing maximum intensity of the curve should be related to the vaporization position of the particle. Therefore, by measuring the position, the time for complete vaporization can be estimated. For particle sizes of 0.35 and 1.4μm, the change in signal intensity with variation of observation height shows the same trend as that of the 2.5 μm particle, as shown in Fig. 6. From this figure, it can be seen that higher signals were obtained as the particle size decreased. This is to be expected because smaller sized particles should have a better analyte transport efficiency and subsequent vaporization/atomization efficiency. The observation height for the maximum intensities of the slurries decreased as the particle size decreased and reached a minimum for aqueous solution. This result corresponds to the relationship between residence time and particle size. The smaller particle size required a shorter residence time, which led to a lower observation height, regardless of nebulization efficiency. Therefore, the maximum intensity of the 2.5 μm particle, *i.e.*, the largest, was obtained at an observation height of 14.2 mm, while the maximum intensities of the 1.4 μm and 0.35 μm particles were estimated to be at heights 12.7 mm and 12.0 mm, respectively. The aqueous solution shows the lowest observation height, as expected. From Fig. 5, regardless of particle size, the maximum signal intensity of the slurry particles never reached the value of the aqueous solution, even though the 0.35 and 1.4 μm particles were very small. As long as particles are not vaporized instantly in the plasma, a wider distribution is expected for a vaporized droplet than for aqueous solution, which leads to a smaller signal intensity for the slurry particle. Results of similar experiments have been shown in previously published papers.[21,22]

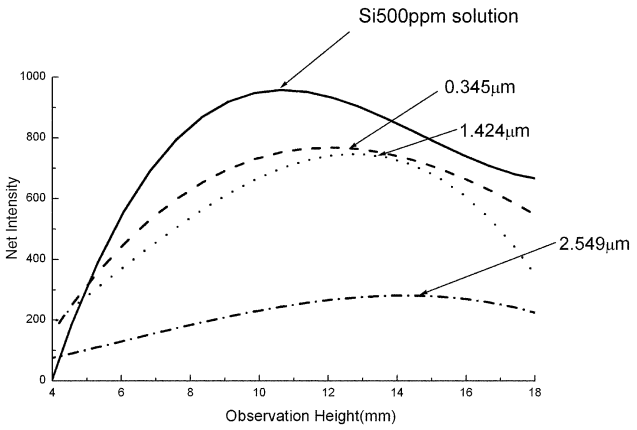

Fig. 6 Intensity change of SiO_2 particles at 0.35, 1.4, and 2.5 μm, and an aqueous sample, when the observation height was varied.

Calculation of vaporization constant

Since the complete vaporization time is measured with difficulty, the differences in the observation heights producing maximum intensity were measured. The difference can be regarded as the result of the difference in the vaporization time for different particle sizes vaporized in the plasma. Currently, these experimental differences in the observation height can be compared with those of the vaporization time and distance, calculated by theory based on particle desolvation and the vaporization mechanism. From this comparison, we can deduce which desolvation and vaporization mechanisms in the ICP can be applied for a prepared SiO_2 slurry particle.

The calculation of the difference in observation height in the ICP was performed based on the method and mechanism proposed by Hieftje and co-workers.[10,11] They found that the desolvation rate for water was a linear function of the time spent by the droplet in the flame. According to their theory, desolvation occurs at a rate limited by mass transfer during the period when the surface temperature of the droplet is lower than the boiling point of the solvent. The desolvation process occurs by heat-transfer-limited kinetics, while the surface of the droplet is at the boiling point. A similar study was conducted by Raeymaekers *et al.*[2] Raeymaekers *et al.* accepted heat-transfer-controlled evaporation of the refractory particles and included the velocity and residence time of the analyte, but did not consider a possible turnover from heat-transfer to mass-transfer control.

In our study, three mechanisms, heat-transfer-controlled, mass-transfer-controlled, and Knudsen-effect-corrected heat-transfer-controlled vaporization,[11] were considered for SiO_2 slurry particles.

For the mass-transfer-controlled vaporization mechanism, the following equation was used:

$$t=[(\frac{2-\alpha}{\alpha})(r_o-r)+(\frac{v}{D})(r_o^2-r^2)][\frac{(2\pi MRT_g)^{1/2}\rho}{2MP_s}] \qquad (3)$$

From the equation, the changes in the physical parameters, for example, the thermal properties, caused changes in the theoretical results of the vaporization process. The symbols in the equation and physical parameters used in the calculation are listed in Table 2. The importance and meaning of the parameters were explained in a paper previously published by Hieftje *et al.*[11] In our experiments, the particles to be vaporized were different sizes of SiO_2 particles.

The thermal conductivity and heat capacity of the solute vapor were evaluated at T_g because the temperature will eventually become the same as that of the plasma gas. Because of the difficulty in obtaining an accurate thermal conductivity of SiO_2, it was calculated at the plasma temperature by considering the mass and thermal conductivity of Ar. The temperature of the plasma was estimated from data published by Raeymaekers *et al.*[2] The surface temperature of the SiO_2 particle, T_s, was at the boiling point and the saturation vapor pressure of the SiO_2 particle at the surface, P_s, was equal to that of the Ar plasma at 1 atm.

For the theoretical treatment in our experiments, the vaporization coefficient in eqn. (3) for mass-transfer-controlled vaporization varied from 0.01 to 0.5. In this process, the particle vaporization rate constant, k, was obtained followed by calculation of the observation height in the plasma for complete vaporization. The results of the difference in the observation height for different sizes of particles are listed in Table 3. The gas flow rate of the plasma in this experiment was assumed to be 20 m s^{-1}. As shown in Table 3, the larger the vaporization coefficient, α, the smaller the difference in

Table 2 Physical parameters for the calculation of the vaporization process for SiO_2 particles

Parameter	Units	Note
λ: thermal conductivity	1.589×10^{-4} cal s^{-1} cm^{-1} K^{-1}	Assumed
C_p: heat capacity	85.772 J K^{-1} mol^{-1}	
ρ: density[a]	1.77 g cm^{-3}	Assumed
T_g: temperature of plasma	5000 K	Assumed (ref. 2)
T_s: temperature of surface (bp)	2863 K	
H_v: heat of vaporization[b]	143.4 kcal mol^{-1}	
Z^*: temperature-jump distance	2.35 μm	Assumed
α: evaporation coefficient	0.01–0.4	
P_s: saturation vapor pressure	1.013×10^6 dyn cm^{-2}	
R: gas constant	8.16×10^7 dyn cm K^{-1} mol^{-1}	
D: diffusion coefficient[c]	5 cm^2 s^{-1}	Assumed
Λ: mass counterflow coefficient	0.873	Calculated

[a] ρ: assumed at the particle boiling point, T_s. [b] H_v: assumed to be the same as the enthalpy of sublimation. [c] D: assumed at the particle boiling point, T_s.

Table 3 Comparison of measured and calculated observation height differences for complete particle vaporization, with variation of vaporization coefficient, α

		Calculated distance between maximum intensities/mm					
Particle size/μm	Experimental distance/mm	$\alpha=0.01$	$\alpha=0.1$	$\alpha=0.2$	$\alpha=0.3$	$\alpha=0.4$	$\alpha=0.5$
0.35							
	0.71	39	3.9	1.9	1.2	0.90	0.70
1.45							
	1.5	41	4.2	2.1	1.4	1.1	0.88
2.55							

observation height for different sized particles. If α is small, most of the vaporization of the SiO_2 particles would fall into the small particle category. Reportedly,[23] when α assumed the values of 0.01 and 0.2, the critical radius for NaCl in a flame was calculated to be 4.8 and 0.19 μm, respectively. Compared with the values for NaCl, the value of α for a SiO_2 particle is too large for a mass-transfer-controlled mechanism. For our experiments, α should be larger than 0.4 for the calculated observation height distance to correspond with the experimental distance. Because of this, a mass-transfer-controlled vaporization mechanism was not considered feasible for SiO_2 slurry particles in an Ar plasma.

For calculation involving the heat-transfer-controlled and Knudsen-effect-corrected heat-transfer-controlled vaporization mechanisms, the following equations were used (additional parameters are listed in Table 2):

$$r_0^2 - r^2 = \left[\frac{2M\Lambda\lambda(T_g - T_s)}{\Delta H_v \rho}\right] t = k_{v1} t \quad (4)$$

$$r_0^2 - r^2 = \left[\frac{2M\Lambda\lambda(T_g - T_s)}{\Delta H_v \rho}\right] t - 2Z^*(r_0 - r) \quad (5)$$

In the above equations, the mass counterflow coefficient was calculated. In ICP, the heat-transfer calculation takes account of the Knudsen effect because the Knudsen number, K_n, can be an intermediate value. In order to consider the Knudsen effect, effective temperature-jump distance, Z^*, should be involved. For the calculation of Z^*, the thermal accommodation coefficient was assumed to be 0.8, and has the same assumption value as the evaporation coefficient, α, as discussed by Hieftje *et al.*[11]

The calculated results for the differences in observation heights are shown in Table 4. The calculated differences in observation height, which produce the maximum intensity using the Knudsen-effect-corrected heat-transfer mechanism, were too large compared with those obtained by experiment. This means that the radius of the particle decreases very slowly with time for SiO_2 under the Knudsen-effect-corrected heat-transfer-controlled model, and the calculated vaporization rate of the process is smaller than that obtained experimentally. The differences in the mass-transfer and heat-transfer mechanisms are closer to the experimental distances. For the mass-transfer mechanism, as previously mentioned, the vaporization coefficient was unexpectedly high; the difference between 0.35 and 1.4 μm is close enough but not the distance between 1.4 and 2.5 μm. The values calculated by the heat-transfer model in both size ranges were relatively close to those obtained by experiment, indicating that SiO_2 particles are vaporized *via* the heat-transfer mechanism rather than the Knudsen-effect-corrected heat-transfer or mass-transfer mechanisms. As a result, when the heat-transfer-controlled model is considered for the vaporization process, the vaporization rates for the SiO_2 particles of sizes 0.35 μm, 1.4 μm and 2.5 μm become the most

Table 4 Comparison of measured and calculated results from different sized SiO_2 particles

			Calculated distance between maximum intensities/mm		
Particle size/μm	Max. intensity height/mm	Experimental distance/mm	Heat transfer, k_{v1}, 1.4×10^{-4} cm^2 s^{-1}	Knudsen-effect corrected	Mass transfer $\alpha = 0.5$
0.35	12.0				
		0.7	0.68	4.3	0.70
1.4	12.7				
		1.5	1.6	5.4	0.88
2.5	14.2				

comparable to those obtained by experiment in an atmospheric pressure ICP.

In conclusion, it was proved that SiO_2 particles in the range of 0.3–2.6 μm vaporized *via* the process of a heat-transfer-controlled mechanism, rather than that of the Knudsen-effect-corrected heat-transfer-controlled and the mass-transfer-controlled mechanisms.

Acknowledgement

This work was supported by Grant 1999-2-124-001-5 of the Interdisciplinary Research Program, KOSEF.

References

1 D. C. Gregoire, N. J. Miller-Ihli and R. E. Sturgeon, *J. Anal. At. Spectrom.*, 1994, **9**, 605.
2 B. Raeymaekers, T. Graule, J. A. C. Broekaert, F. Adams and P. Tschopel, *Spectrochim. Acta, Part B*, 1988, **43**, 923.
3 L. Ebdon, M. Foulkes and K. O'Hanlon, *Anal. Chim. Acta*, 1995, **311**, 123.
4 L. Ebdon, M. E. Foulkes, H. G. M. Parry and C. T. Tye, *J. Anal. At. Spectom.*, 1988, **3**, 753.
5 A. J. Ambrose, L. Ebdon, M. E. Foulkes and P. Jones, *J. Anal. At. Spectrom.*, 1989, **4**, 219.
6 R. Guevremont and K. Nimalasiri De Silva, *Spectrochim. Acta, Part B*, 1991, **46**, 67.
7 P. Goodall, M. E. Foulkes and L. Ebdon, *Spectrochim. Acta, Part B*, 1993, **48**, 1563.
8 C. Chen and T. W. McCreary, *Appl. Spectrosc.*, 1994, **48**, 410.
9 L. Halicz, Isaac B. Brenner and O. Yoffe, *J. Anal. At. Spectrom.*, 1993, **8**, 475.
10 G. J. Bastiaans and G. M. Hieftje, *Anal. Chem.*, 1974, **46**, 901.
11 G. M. Hieftje, R. M. Miller, Y. Pak and E. P. Wittig, *Anal. Chem.*, 1987, **59**, 2861.
12 N. C. Clampitt and G. M. Hieftje, *Anal. Chem.*, 1972, **44**, 1211.
13 J. A. Horner and G. M. Hieftje, *Spectrochim. Acta, Part B*, 1998, **53**, 1235.
14 J. C. Giddings, *Sep. Sci. Technol.*, 1985, **20**, 749.
15 R. Keil, E. Tsamakis, C. B. Fuh, J. C. Giddings and J. I. Hedges, *Geochim. Cosmochim. Acta*, 1994, **58**, 879.
16 C. Contado, F. Riello, G. Blo and F. Dondi, *J. Chromatogr. A*, 1999, **845**, 303.
17 M. H. Moon, D. J. Kang, D. W. Lee and Y. S. Chang, *Anal. Chem.*, 2001, **73**, 693.
18 C. B. Fuh, *Anal. Chem.*, 2000, **72**, 266A.
19 L. Ebdon and A. R. Collier, *J. Anal. At. Spectrom.*, 1988, **3**, 557.
20 J. C. Farinas, R. Moreno and J. M. Mermet, *J. Anal. At. Spectrom.*, 1994, **9**, 841.
21 J. H. Hyun, H. B. Lim and C. H. Lim, *Anal. Chim. Acta*, 1997, **342**, 83.
22 J. G. Choi, H. Y. Kim and H. B. Lim, *Microchem. J.*, 1999, **63**, 119.
23 G. M. Hieftje, R. M. Miller, Y. Pak and E. P. Wittig, *Anal. Chem.*, 1987, **59**, 2861.